# ABOUT THE IMPACT OF WIND TURBINE WAKE VORTICES ON HELICOPTER TRIM AND ROTOR BLADE MOTION

**Berend G. van der Wall** berend.vanderwall@dlr.de
**Paul H. Lehmann** paul.lehmann@dlr.de
German Aerospace Center (DLR), Institute of Flight Systems
Lilienthalplatz 7, 38108 Braunschweig, Germany

**Abstract**

With increasing numbers of large wind turbines on-shore and off-shore, interactions of their wake with helicopters become interesting. In this paper the wake is modeled as a tip vortex helix with a vortex strength estimated from the wind turbine thrust. Helicopter rotors of different size are subjected to the wake and the collective and cyclic controls required to keep the trim are compared to the maximum available controls of the rotorcraft. In addition the blade flapping response due to the vortex influence without pilot action is computed and compared to maximum flapping angles allowed. It is found that typical onshore wind turbines could be a hazard for ultralight helicopters, but not for larger helicopters. Large offshore wind turbines, however, could even be a danger for small helicopters that may be used for maintenance. In addition the results are compared to fixed-wing wake vortex interaction with a helicopter as given in the literature.

## NOMENCLATURE

| | |
|---|---|
| $A, B$ | Non-dimensional effective begin and end of rotor blade, referenced to $R$ |
| $c, c_{eq}$ | Airfoil chord and equivalent chord, m |
| $C_{l\alpha}$ | Lift curve slope |
| $C_T$ | Thrust coefficient of the helicopter rotor |
| $c_n$ | Radial integral coefficients, $n = 0,1,2,$ ... |
| $L, \overline{L}$ | Blade lift, N; non-dimensional blade lift |
| $M_\beta, \overline{M_\beta}$ | Aerodynamic flap moment about the flapping hinge, Nm; non-dimensional flap moment |
| $N_b$ | Number of rotor blades |
| $r$ | Non-dimensional radial coordinate, referenced to $R$ |
| $R_c, r_c$ | Vortex core radius, m; non-dimensional core radius, referenced to $R$ |
| $R, R_{WT}$ | Helicopter and wind turbine rotor radius, m |
| $RCR$ | Rotor control ratio |
| $RFR$ | Rotor flapping ratio |
| $u, v, w$ | Velocity components in $x, y, z$ directions, m/s |
| $U$ | Rotor blade tip speed, m/s |
| $v_{iV}$ | Wake vortex induced velocity, m/s |
| $V_T, V_P$ | Non-dimensional velocities acting tangential and normal at the blade element, referenced to $U$ |
| $V_W$ | Wind speed, m/s |
| $V_\infty$ | Helicopter flight speed, m/s |
| $x, y, z$ | Non-dimensional hub-fixed coordinates of the helicopter rotor, $x$ pos. downstream, $y$ pos. starboard, $z$ pos. up, referenced to $R$ |
| $y_0$ | Vortex position within the rotor disk; non-dimensional, referenced to $R$ |
| $\beta, \beta_0,$ $\beta_C, \beta_S$ | Rotor blade flapping angle, mean, and cyclic components, deg |
| $\beta_V$ | Core radius shape factor |
| $\Gamma, \Gamma_{eq}$ | Wind turbine tip vortex and equivalent straight line vortex circulation strength, m²/s |
| $\Delta$ | Perturbation of a variable |
| $\Theta, \Theta_0,$ $\Theta_C, \Theta_S$ | Rotor blade pitch angle, collective, lateral and longitudinal control angle, deg |
| $\lambda_i$ | Thrust-induced inflow velocity normal to the rotor disk, non-dimensionalized by $U$ |
| $\lambda_V,$ $\lambda_{V0}$ | Wind turbine wake vortex induced inflow ratio and its amplitude, normal to the rotor disk, non-dimensionalized by $U$ |
| $\mu$ | Rotor advance ratio, $\mu = V_\infty / U$ |
| $\nu_\beta$ | Natural frequency of flapping, non-dimensionalized by $\Omega$ |
| $\rho$ | Air density, kg/m³ |
| $\sigma$ | Rotor solidity, $\sigma = N_b c/(\pi R)$ |
| $\psi$ | Rotor blade azimuth, deg |
| $\psi_V$ | Wake age in terms of azimuth behind the blade, deg |
| $\Omega, \Omega_{WT}$ | Rotor rotational speed of helicopter rotor and wind turbine, rad/s |

## 1. INTRODUCTION

In past decades the effects of rotorcraft encountering the wake vortex of large fixed-wing aircraft as sketched in Fig. 1 have been a subject of interest. This may happen in military operations with large transport aircraft and utility helicopters, but also heliports in the vicinity of airport runways may be subjected to large civil aircraft wake vortices. In the 1980s, NASA [1] and US Army [2] investigated a UH-1H helicopter trimmed at 60 kts flying through the wake vortices of a Douglas C-54 airplane at varying distances. Over the range of 0.42 nm to 6.64 nm, maximum rotor blade structural loads, helicopter attitude response and tail rotor flapping were measured, the helicopter reactions were recognized but did not constitute safety hazards.

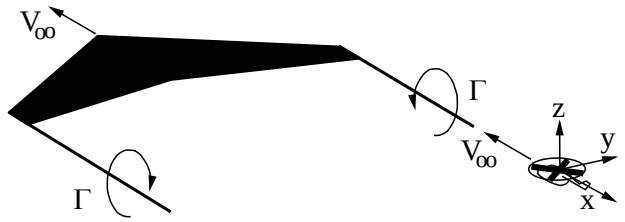


( a ) Sketch of a fixed wing wake with a helicopter

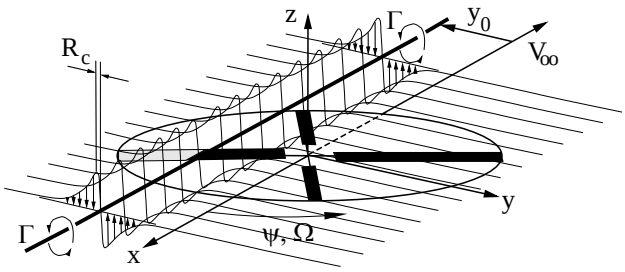


( b ) Helicopter rotor with a single straight vortex

**Fig. 1:** Fixed wing vortex - rotor interaction.

Numerical simulation was used in [3] and [4] to investigate the effects from a pair of trailing vortices of a preceding large Boeing 747 (B-747) airplane on the flight dynamics of a fixed and a rotary wing aircraft. The responses of airplane and helicopter are described as different in a way that the helicopter reacts more damped to the disturbance by the tip vortex.

More recently, work has been conducted by the University of Liverpool and QinetiQ, [5]-[7]. They investigated the influence of an active runway from an international airport to helicopter operations from a nearby approach and takeoff area. For their work they used flight mechanics simulation tools to examine the effects when a helicopter encounters the shed tip vortex from a large aircraft.

A model of the vortex velocity profile was established by the use of LIDAR measurement data from the airport. Several calculations for the Lynx helicopter in forward speeds from hover to 80 kts were conducted. The results showed that the helicopter reaction is primarily dependent on the rotor position relative to the vortex center. In some combinations, hazardous helicopter reactions were recognized. The main question is, whether a rotorcraft which meets handling performance standards is able to recover the disturbed flight attitude after encountering the vortex.

The rotor blade and helicopter response to vortex encounters was numerically investigated in [8] and [9], emphasizing the mutuality of the interaction. It was concluded that the interacting vortex deformation under rotor airloads significantly reduces the impact on rotor and helicopter response, compared to a rigid vortex and an unidirectional interaction.

Today another source of rotorcraft-vortex encounter is emerging: more than 27000 on-shore wind turbines (WT) in Germany (end of 2016) with up to 7.5 MW power often are in the vicinity of the numerous glider and sport aircraft airfields. Ultralight autogyros are flying in large numbers in Germany since 2009 and ultralight helicopters regulations were recently established (Dec. 2016) and are to be expected also to enter the market in large numbers. Off-shore wind farms consist of WT having 5 to 8 MW power and larger ones being planned. For maintenance small helicopters are used that will encounter the wakes of such WT. In addition, the interaction of ultralight rotorcraft with WT wake vortices as sketched in Fig. 2 is an emerging subject of interest as well. A first paper on the subject was presented by the authors in [10].

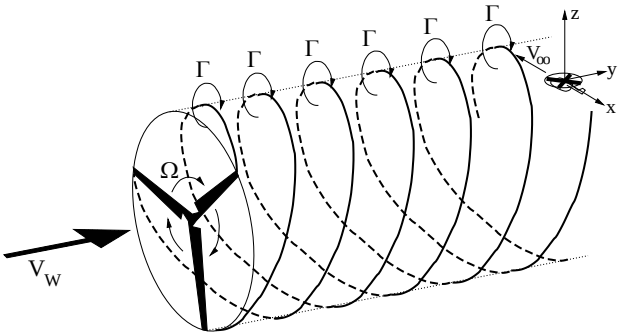


( a ) Sketch of a WT wake with a helicopter

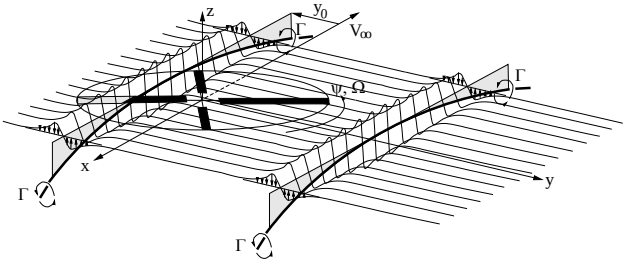


( b ) Helicopter rotor in a curved WT wake with multiple vortices

**Fig. 2:** Wind turbine vortex - rotor interaction.

Such horizontal axis WTs have a downstream wake which is characterized by a spiral helix of usually three blade tip vortices on the surface of the wake tube, as the number of blades is three for the overwhelming majority of the installed systems, see Fig. 2 (a).

The tip vortex spiral on the surface of the tube is fed with circulation from the WT blades. Around each of these vortices induced swirl velocities are generated that are oriented towards the turbine inside the tube – resulting in a global wind deficit – and adding on the wind velocity outside the tube.

Thus, inside the tube a global “wind deficit” is present that manifests itself as a loss of air momentum. Crossing the tube horizontally at half of its height will

therefore generate a side-slip angle for the aircraft when penetrating the wake tube boundary on one side. This side-slip angle vanishes again when penetrating the wake tube boundary on the opposite side. When entering the boundary of the wake large horizontal vortex swirl velocities are encountered that change their sign at the boundary itself, representing a dual lateral pulse for the aircraft.

The situation is very different when crossing the wake tube at its upper or lower boundary, i.e. in the immediate vicinity of the center of these vortices as indicated in Fig. 2 (a), showing the staggered vortices of the wake spiral and a helicopter approaching it from the right. The interactional problem of a helicopter rotor with four individual rotor blades passing the upper end of the wake spiral in almost normal direction to it is shown in Fig. 2 (b). In general this problem is unsteady because the rotating blades enter and pass the WT tip vortex induced velocity field periodically during their revolution.

The curvature of the WT wake spiral within the rotor is very small and can be ignored, because the WT radius is more than 10 times of the ultralight rotor radius, which reduces the problem to that shown in Fig. 1 (b) with a straight vortex. An analytical closed-form estimate to compute rotor controls required for rejection of the vortex disturbance by means of a simplified blade element method was derived in [11] for the first time in the literature. In this paper it will be extended to the rotor blade flapping response when no pilot action is employed.

## 2. DESCRIPTION OF THE MODELS

### 2.1. The wind turbines and the wake model

The investigations of this paper focus on two WT of different power class: a representative on-shore 3 MW turbine and a representative off-shore 7 MW turbine. The reference chord at 93% radius is used to define the initial tip vortex core radius, while the equivalent solidity of the WT rotors is based on the thrust-weighted chord distribution. Data for the WT are given in Table 1. The “worst case” scenario is of interest, which is the operational condition of the WT with maximum tip vortex circulation strength which can be estimated from the rotor thrust coefficient.

The computation of the maximum circulation strength is outlined in [12] and not repeated here. It must be noted that the rotational speed as function of the wind speed is not revealed by the manufacturers and thus had to be estimated by the authors. Also, the thrust curve of the 7 and 10 MW WT is unknown and therefore the same thrust coefficient as for the 3 MW turbine was used instead. The WT wake-induced velocities are computed numerically at distances up to four WT rotor radii behind the turbine, and around distances centered at 500 m behind it.

**Table 1:** Vortex generator data (10 MW estimated).

| Generator: | 3 MW | 7 MW | 10 MW | B-747 |
|---|---|---|---|---|
| $R$, m | 56.5 | 77.0 | 95.0 | 29.8 |
| $\Gamma_0$, m²/s | 63.7 | 98.6 | 130 | 660 |
| $c(0.9R)$,m | 1.000 | 1.363 | 1.682 | 5.070 |
| $R_{c0}$, m | 0.050 | 0.068 | 0.084 | 0.253 |

The wake is represented by eight revolutions of each blade’s wake (beginning at the turbine in the first case, centered about the mean distance in the second case). Every revolution is discretized by 72 straight line vortex elements, each one representing a 5 deg increment. Induced velocities of these finite-length straight vortex elements, including a core radius model, are computed numerically.

The swirl velocity profile includes a core radius $r_c$, a lateral position within the rotor disk $y_0$ and the swirl velocity magnitude depends on the vortex circulation strength $\Gamma$. Coordinates $x, y, z$ and lengths such as the core radius and vortex location within the rotor disk are made non-dimensional by the helicopter rotor radius $R$, velocities are referred to the tip speed $U = \Omega R$ to provide the wake-induced inflow ratio $\lambda_V$ as fraction of the helicopter blade tip speed. The circulation is made non-dimensional by division through $UR$. For an analytical solution of the problem sketched in Fig. 1 (b) the WT vortex within the rotor disk is replaced by an equivalent infinitely long straight line vortex with an associated equivalent circulation $\Gamma_{eq}$ as sketched by the dashed line in Fig. 3.

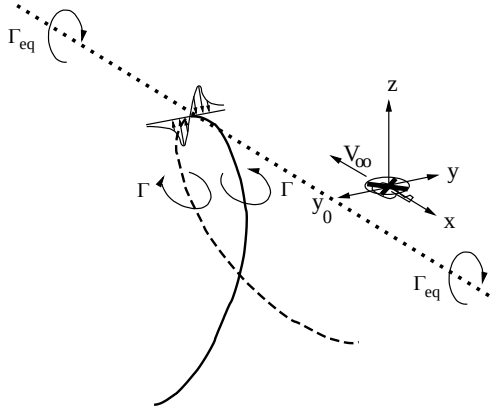


**Fig. 3:** Replacement of the WT spiral vortex by an infinite long straight line vortex.

This straight line vortex is modeled with a core radius model of Burnham-Hallock [13], which is a special case of the Vatistas’ model [14]. The equivalent circulation $\Gamma_{eq}$, or the inflow ratio $\lambda_{V0}$, are then estimated based on the computed wake-induced velocity profiles. It turns out that for the cases investigated here this equivalent circulation is about half of the value of the WT spiral vortex strength.

$$\lambda_V = \frac{v_{iV}}{U} = \frac{\Gamma_{eq}}{2\pi UR}\frac{y-y_0}{\left(y-y_0\right)^2 + r_c^{\,2}}$$

(1)

$$= \lambda_{V0}\frac{r\sin\psi - y_0}{\left(r\sin\psi - y_0\right)^2 + r_c^{\,2}}; \quad \lambda_{V0} = \frac{\Gamma_{eq}}{2\pi UR}$$

The peak value of the inflow ratio is obtained at the core radius itself.

(2) $$\lambda_{V,max} = \frac{\lambda_{V0}}{2r_c} = \frac{\Gamma_{eq}}{4\pi UR_c} = \frac{V_c}{U}$$

Natural diffusion is represented by time-dependent decay (or aging) functions for both the circulation strength (which reduces asymptotically to zero for long time) and the vortex core radius (which widens with time) in the manner following [13] and [15].

(3) $$r_c = \frac{R_{c0}}{R}\sqrt{1+\frac{5\cdot 10^{-6}\,rad/s}{\left(R_{c0}/R_{WT}\right)^2\Omega_{WT}}\psi_v}$$

$$\Gamma = \Gamma_0 e^{-0.001932\psi_V}$$

The initial core radius $R_{c0}$ is set to 5% of the WT blade chord length at 93% radius (i.e., the reference chord at the blade tip area). Both decay factors of the core radius and the circulation aging functions are empirical, based on measurements.

While the Vatistas model is used in the analytical isolated rotor investigations the "Helicopter Overall Simulation Tool" (HOST, [16]) makes use of another formulation, the "Atmospheric Environment Submodule" (AES). This submodule is connected to HOST's flight mechanics model, calculates disturbed air and provides all relevant helicopter parts with the related turbulence parameters. The AES is able to simulate the following types of wake: atmospheric turbulence, big size aircraft vortex wake model, gusts in all directions, and the flow around different types of buildings. Here it is used with the big size aircraft wake vortex. The influence of the helicopter's thrust-induced velocity on the aircraft vortex motion is not modelled.

All calculations performed here were conducted with the flight mechanics model of the BO105 helicopter and the so-called "Big Size Aircraft Vortex Wake Model". Therein, the vortices are described following the Lamb-Oseen formula [17], [18]. Its equivalent circulation strength or swirl velocity $V_c$, a core radius $R_c$ and a decay factor $\beta_V$ must be provided; they are estimated from the computed WT wake-induced velocity field. At a distance $y = 0$ from the core center this formula has a numerical singularity, but it can be proven that the analytical boundary value results in $v_V = 0$, because the expression in brackets of Eq. (4) approaches the zero faster than the division by $y$.

(4) $$\lambda_V = \frac{v_{iV}}{U} = \frac{V_c}{U}\frac{R_c}{y}\left[1 - e^{-\beta_V\left(\frac{y}{R_c}\right)^2}\right]$$

$$\lambda_{V,\max} = 0.638\frac{V_c}{U}; \quad y\left(\lambda_{V,\max}\right) = 1.1209R_c$$

Note that for the value used of $\beta_V = 1.0$ the maximum swirl velocity is $v_{iV,max} \approx 0.638V_c$, obtained at $y \approx 1.12R_c$.

Three cases A, B and C representing a vortex of a 3, 7 or a 10 MW WT in a distance of 100 m are investigated, larger distances are considered less important due to vortex aging. Therefore the HOST airplane wake model is provided with the data given in Table 2 for these cases. The fourth case D represents a vortex trailed by a B-747 aircraft 2 km behind it, as used in [4], also considered a young and thus most intense vortex. For these cases the vortex-induced velocity distributions for both models based on Eq. (1) and Eq. (4) are shown in Fig. 4.

**Table 2:** Properties of the HOST big size aircraft vortex wake model and for the Vatistas' model.

| | WT, MW | Dist., km | HOST $R_c$, m | HOST $V_c$, m/s | Vatistas $R_c$, m | Vatistas $V_c$, m/s |
|---|---|---|---|---|---|---|
| A | 3 | 0.1 | 0.415 | 10.3 | 0.393 | 6.18 |
| B | 7 | 0.1 | 0.568 | 11.6 | 0.542 | 7.00 |
| C | 10 | 0.1 | - | - | 0.646 | 7.76 |
| D | B-747 | 2.0 | 3.345 | 26.5 | 3.280 | 16.0 |

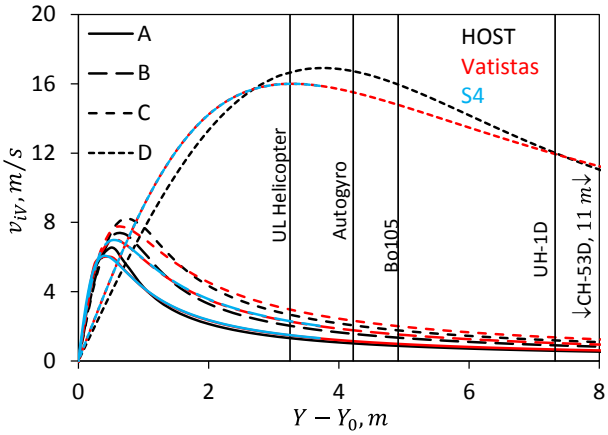


**Fig. 4:** Induced velocity distributions for cases A-D of Table 2 in relation to various helicopter rotor radii.

Although the formulae are quite different, the resulting velocity profiles are rather close to each other and allow a direct comparison of HOST results with the analytical model. The rotor radii of various rotorcraft vehicles are indicated in the figure as well in

order to give an impression of the vortex size relative to the radius of the encountering vehicle. It is also obvious from Fig. 4 that the WT vortices seem unimportant for large helicopters like the CH-53, but already important for UL-helicopters and autogyros, especially considering the smaller tip speed of those compared to larger helicopters. The B-747 vortex appears huge for the smaller rotorcraft, and for the UL helicopter represents almost a linear variation of normal velocity across its disk with about twice of its mean thrust-induced velocity at the core radius.

## 2.2. Rotor Models

### 2.2.1. The HOST helicopter model

For flight mechanics purposes the Institute of Flight Systems at DLR uses HOST [16] for desktop simulation, which was developed by Airbus Helicopters. It is a modular tool that has the ability to simulate any type of helicopter and to calculate trim, time domain response and other. For the results obtained here HOST was used in a special configuration with an isolated rotor trim instead of a complete helicopter trim in combination with the aforementioned "Big Size Aircraft Vortex Wake Model". It is assumed that this wake model is able to represent the idealized vortex in the wake of a WT while it is provided with the required vortex data core radius and swirl speed at the core radius as given in Table 2.

The helicopter model used for these investigations, the Bo105, is a light utility rotorcraft with a mass of 2200 kg representative for those used in maintenance of offshore wind farms. The HOST model assumes an articulated rotor with rigid blades flapping about an effective hinge offset with a spring and the Meier-Drees model [19] is used for the induced velocity calculation due to rotor thrust.

### 2.2.2. DLR's S4 rotor simulation code

S4 is a high-resolution isolated rotor comprehensive simulation code described in detail in [20]. A Bo105 full-scale elastic rotor blade model is used with two flapping and one lag modes. Nonlinear steady aerodynamics and constant inflow are used for this study for comparison with HOST and with the analytical rotor model described in the following section. The rotor blade is discretized into 40 blade elements and 2 deg azimuth steps are used for time-marching numerical integration of the modal equations of motion to solve the dynamic response problem.

A finite length straight line vortex that can be arbitrarily oriented with respect to the rotor was implemented into the S4 code. To compute all three components of the vortex-induced velocities at all blade elements instantaneous positions a core radius and the Biot-Savart law is used. As shown in Fig. 4 this vortex model essentially represents a Vatistas type of velocity profile.

### 2.2.3. The analytical rotor model

Based on the sketch of Fig. 1 (b) the velocities acting on a rotor blade element tangential (in the rotational plane, normal to the radial axis) and normal to the rotational plane can be established. It is assumed that:

- the helicopter's flight path is parallel to the WT's wake vortex axis,
- the vortex center lies in the plane of the rotor disk,
- the rotor is horizontal.

Then, as indicated in the sketch, only vertical vortex-induced velocities are acting on the blade elements and they are a function of the lateral coordinate $y$ only. All velocities can be split into those components present in an isolated rotor (index 0) and those components due to the WT wake $\lambda_V$ from Eq. (1) that are considered as perturbations (Δ values).

The in-plane velocity $V_T$ acting at a blade element consists of the circumferential velocity expressed by $r$ and the contribution of the advance ratio $\mu$. Contributions to the normal velocity come from the inflow ratio due to forward flight $\mu_z$, the thrust-induced inflow ratio $\lambda_i$, the WT vortex-induced inflow ratio $\lambda_V$, and due to rotor blade flapping position $\beta$ as well as due to flapping motion $d\beta/d\psi$.

$$V_T = r + \mu \sin\psi \quad = V_{T0} + \Delta V_T;\ \ \Delta V_T = 0$$

$$V_P = \mu_z + \lambda_{i0} + \Delta\lambda_i + \lambda_V + \mu\beta\cos\psi + r\,d\beta/d\psi \tag{5}$$

$$= V_{P0} + \Delta\lambda_i + \Delta V_{PV} + \Delta V_{P\beta}$$

A trim of the rotor requires collective control $\Theta_0$, longitudinal $\Theta_S$ and lateral cyclic control angles $\Theta_C$ in order to establish the required thrust, propulsive and lateral forces, as well as the hub moments needed for a steady flight. Any perturbations of the velocities acting at the blades therefore require perturbations in the controls ΔΘ in order to maintain the trim. Rotor blade flapping can also be considered to consist of a flapping motion resulting in trim $\beta$ and a perturbation $\Delta\beta$ caused by the vortex.

$$\begin{aligned} \Theta &= \Theta_0 + \Theta_S \sin\psi + \Theta_C \cos\psi \\ \Delta\Theta &= \Delta\Theta_0 + \Delta\Theta_S \sin\psi + \Delta\Theta_C \cos\psi \\ \beta &= \beta_0 + \beta_S \sin\psi + \beta_C \cos\psi \\ \Delta\beta &= \Delta\beta_0 + \Delta\beta_S \sin\psi + \Delta\beta_C \cos\psi \end{aligned} \tag{6}$$

For simplification a perturbation parallel to the $x$-axis is assumed (see Fig. 1 (b)), which causes only lateral unbalance of vortex-induced inflow. In longitudinal direction the disturbances are always balanced fore and aft of the rotor hub, thus $\Delta\Theta_C = 0$.

The governing equation of rotor blade flapping for trim and perturbations is given by Eq. (7), including the natural frequency of flapping $\nu_\beta$ and the blade Lock number $\gamma$. Like the flapping angle, the aerodynamic moment $\overline{M_\beta}$ can be split into a trim value plus perturbations in the mean and 1/rev components.

$$\begin{aligned} d^2\beta/d\psi^2 + \nu_\beta^2\beta &= \gamma\overline{M_\beta} \\ d^2\Delta\beta/d\psi^2 + \nu_\beta^2\Delta\beta &= \gamma\,\Delta\overline{M_\beta} \end{aligned} \tag{7}$$

The blade section angle of attack is defined by three contributions: first, the pitch angle Θ, which is needed for the helicopter trim in undisturbed atmosphere. Second, a perturbation ΔΘ (Eq. (6)) to compensate the trim disturbance caused by the third contribution, namely the WT vortex-induced velocities given in Eq. (5). First, this results into an equation for the steady (mean) lift perturbation to be zero. Second, the $1/\mathrm{rev}$ aerodynamic flapping moment perturbation about the hub must be zero as well. Both of these values require a radial integration of the section lift distribution from the effective begin of the airfoiled part of the blade $A$ to the effective end of it $B$. Lift and moment are referenced to $\rho(\Omega R)^2 cRC_{l\alpha}$ and $\rho(\Omega R)^2 cR^2 C_{l\alpha}$, respectively.

$$\begin{aligned} \Delta\overline{L} &= \int_A^B \Delta\overline{dL} \approx \frac{1}{2}\int_A^B V_T^2\left(\Delta\Theta - \frac{\Delta V_P}{V_T}\right)dr \\ &= \Delta\Theta_0\,\frac{1}{2}\int_A^B \left(r+\mu\sin\psi\right)^2 dr \\ &+\Delta\Theta_S\,\frac{1}{2}\int_A^B \left(r+\mu\sin\psi\right)^2 \sin\psi\, dr \\ &-\Delta\lambda_i\,\frac{1}{2}\int_A^B \left(r+\mu\sin\psi\right) dr \\ &-\lambda_{V0}\,\frac{1}{2}\int_A^B \frac{\left(r+\mu\sin\psi\right)\left(r\sin\psi - y_0\right)}{\left(r\sin\psi - y_0\right)^2 + r_c^2}\,dr \end{aligned} \tag{8}$$

The equation for the moment is:

$$\Delta\overline{M_\beta} = \int_A^B r\,\Delta\overline{dL} \tag{9}$$

To solve the wake integral of the perturbation lift a Fourier series is needed for ease of further processing. However, a broken rational function with periodic terms in both nominator and denominator is present. A Fourier analysis transforms this into the desired form, [10].

$$\begin{aligned} &\frac{\left(r+\mu\sin\psi\right)\left(r\sin\psi - y_0\right)}{\left(r\sin\psi - y_0\right)^2 + r_c^2} \\ &= a_{V0} + \sum_{i=1}^{\infty}\left(a_{Vi}\cos i\psi + b_{Vi}\sin i\psi\right) \end{aligned} \tag{10}$$

The mean value $a_{V0}$ is needed for keeping the mean value of the lift perturbation zero ($\Delta\overline{L_0} = 0$) and the $1/\mathrm{rev}$ sine part $b_{V1}$ is needed for keeping the rotor roll moment perturbation zero (in the rotating frame that is $\Delta\overline{M_{\beta S}} = 0$), all higher harmonics are of no interest for this study since they do not affect the rotor trim. A rotor pitching moment perturbation is not generated due to the vortex axis being parallel to the rotor $y$-axis (in the rotating frame: $\Delta\overline{M_{\beta C}} = 0$).

### 2.3. Rotors investigated and method applied

Within this study an isolated rotor trim is the basis of analysis. The purpose is to compare HOST results with the analytical model estimates and with DLR's S4 rotor code in order to investigate the differences between these methods.

Various rotors are investigated with respect to the controls required to mitigate the vortex effects and to compute the flapping perturbations when no controls are applied. With respect to on-shore WT interactions, sports ultralight rotorcrafts (UL) are of interest such as autogyros (AG) and coaxial helicopters (COAX). Regarding off-shore WT interaction helicopters of the Bo105 size are of interest. An interaction with a vortex of a wide body aircraft like a B-747 is considered for these rotorcraft and larger ones such as an UH-1D and a CH-53D. Parameters used are given in Table 3; the values for the AG and the UL helicopter are considered as representative.

**Table 3:** Properties of the rotor blades investigated.

| | AG | COAX | Bo105 | UH-1D | CH-53D |
|---|---|---|---|---|---|
| type | see-saw | see-saw | hinge-less | see-saw | articu-lated |
| $R$, m | 4.22 | 3.25 | 4.91 | 7.32 | 11.0 |
| $U$, m/s | 155 | 153 | 218 | 248 | 213 |
| $\gamma$, Lock | 4.84 | 6.22 | 8.00 | 6.53 | 8.91 |
| $\nu_\beta$, /rev | 1.00 | 1.00 | 1.12 | 1.00 | 1.09 |
| $\Delta\Theta_{max}$ | - | 8° | 8° | 8° | 8° |
| $\Delta\beta_{max}$ | 7° | 5.73° | 15° | 12° | 14° |

To determine the perturbation in main rotor control angles due to the aircraft vortex, the rotor is trimmed at prescribed forward speed in the influence area of the vortex. The rotor is positioned in a way that the vortex is in the same height as the rotor hub and is varied in position from $y = -2R$ to $+2R$ in steps of $0.25R$. The perturbation control angles are obtained by subtracting the trim controls of the undisturbed atmosphere (without a vortex) from the trim controls including the vortex.

When the rotor is always trimmed to constant thrust, then $\lambda_i$ is constant and thus $\Delta\lambda_i = 0$. This also implies trimming for constant hub moments which yields rotor blade flapping perturbations in 1/rev will be zero. However, the mean flapping (coning) – despite constant thrust – will slightly vary because

the steady lift radial distribution will vary depending on the vortex position and its properties. Otherwise, when keeping the controls of trim in undisturbed atmosphere fixed and then introducing the vortex, the thrust will change depending on the vortex influence and hence $\Delta\lambda_i \neq 0$ and $\Delta\beta \neq 0$.

### 2.4. Solutions

#### 2.4.1. Constant trim

Constant trim means to keep rotor thrust and hub moments constant by applying collective and cyclic control perturbations. Constant thrust yields $\Delta\lambda_i = 0$ and is expressed by Eq. (11), derived from Eq. (8).

$$\begin{aligned} 0 &= \Delta\Theta_0 \frac{1}{2}\int_A^B \left( r^2 + \frac{\mu^2}{2} \right) dr + \Delta\Theta_S \frac{1}{2}\int_A^B \mu r \, dr \\ &\quad -\lambda_{V0} \frac{1}{2}\int_A^B a_{V0} \, dr \\ &= \Delta\Theta_0 \frac{2c_3 + c_1\mu^2}{4} + \Delta\Theta_S \frac{\mu c_2}{2} - \frac{\lambda_{V0}}{2}\int_A^B a_{V0} \, dr \end{aligned} \tag{11}$$

$$c_i = \int_A^B r^{i-1} dr = \frac{B^i - A^i}{i}$$

Constant hub moments require the 1/rev aerodynamic moments about the hub in the rotating frame to be constant, and these imply that the 1/rev flapping remains constant as well, thus $\Delta\beta_C = \Delta\beta_S = 0$. Three governing equations result: one for the mean lift Eq. (11) and two for the Cosine and Sine part of the moment. With a vortex oriented parallel to the rotor $x$-axis no Cosine moments can develop and thus no controls needed to counteract them, hence $\Delta\Theta_C = 0$, reducing the number of equations to two.

In addition, $\Delta\Theta_C$ does not affect the rotor thrust. From the 1/rev Sine part of the aerodynamic moment the second equation, Eq. (12), is derived from Eq. (9). The vortex-related integrals in Eqs. (11) and (12) were first given in [10] and their result is given in the Appendix A1 and A2.

$$\begin{aligned} 0 &= \Delta\Theta_0 \frac{1}{2}\int_A^B 2\mu r^2 \, dr - \lambda_{V0} \frac{1}{2}\int_A^B r b_{V1} \, dr \\ &\quad + \Delta\Theta_S \frac{1}{2}\int_A^B \left( r^3 + \frac{3\mu^2}{4} r \right) dr \\ &= \Delta\Theta_0 \mu c_3 + \Delta\Theta_S \frac{4c_4 + 3c_2\mu^2}{8} - \frac{\lambda_{V0}}{2}\int_A^B r b_{V1} \, dr \end{aligned} \tag{12}$$

#### 2.4.2. Fixed controls

Now all control perturbations are zero $\Delta\Theta = 0$ and the vortex is introduced into the rotor. The perturbation part of Eq. (7) provides the governing equation for the mean flapping (coning), the longitudinal and the lateral flapping. Recall that now the rotor thrust will vary and thus $\Delta\lambda_i \neq 0$. For the case of zero rotor angle of attack as considered here a linearization about the trim condition can be done:

$$\begin{aligned} \Delta\lambda_i &= \frac{d\lambda_{i0}}{dC_T} \Delta C_T; \quad \lambda_{i0} = \sqrt{\sqrt{\frac{C_T^2}{4} + \frac{\mu^4}{4}} - \frac{\mu^2}{2}} \\ \frac{d\lambda_{i0}}{dC_T} &= \frac{C_T}{\sqrt{8}\sqrt{\sqrt{C_T^2 + \mu^4} - \mu^2}\sqrt{C_T^2 + \mu^4}} \end{aligned} \tag{13}$$

The aerodynamic moment Eq. (9) consists of three parts: one that involved the flapping motion only, one due to perturbations in rotor thrust and one due to the vortex. For fixed controls:

$$\begin{aligned} \Delta\overline{M_\beta} &= -\frac{1}{2}\int_A^B r V_T \Delta V_P \, dr \\ &= -\frac{1}{2}\int_A^B r V_T \left( \mu\Delta\beta\cos\psi + r\frac{d\Delta\beta}{d\psi} \right) dr \\ &\quad -\frac{1}{2}\int_A^B r V_T \Delta\lambda_i dr - \frac{1}{2}\int_A^B r V_T \lambda_V dr \end{aligned} \tag{14}$$

First, the part due to rotor blade flapping is considered and all higher harmonics ignored, because the trim is defined by the constant and 1/rev parts.

$$\begin{aligned} \Delta\overline{M_\beta}(\Delta\beta) &= -\frac{1}{2}\int_A^B r V_T \left( \mu\Delta\beta\cos\psi + r\frac{d\Delta\beta}{d\psi} \right) dr \\ &= -\frac{\mu^2 c_2 - 4c_4}{8} \Delta\beta_C \sin\psi \\ &\quad -\left( \frac{\mu c_3}{2}\Delta\beta_0 + \frac{\mu^2 c_2 + 4c_4}{8}\Delta\beta_S \right)\cos\psi \end{aligned} \tag{15}$$

The second part is due to rotor thrust perturbations.

$$\begin{aligned} \Delta\overline{M_\beta}(\Delta C_T) &= -\frac{1}{2}\int_A^B r V_T \frac{d\lambda_{i0}}{dC_T} \Delta C_T \, dr \\ &= -\frac{c_3 + \mu c_2 \sin\psi}{2} \frac{d\lambda_{i0}}{dC_T} \Delta C_T \end{aligned} \tag{16}$$

This requires a computation of the change in thrust coefficient due to the vortex influence.

$$\begin{aligned} \Delta C_T &= -\frac{\sigma C_{l\alpha}}{2} \frac{1}{2\pi} \int_0^{2\pi}\int_A^B V_T \lambda_V \, dr \, d\psi \\ &= -\frac{\sigma C_{l\alpha}}{2} \lambda_{V0} \int_A^B a_{V0} \, dr \end{aligned} \tag{17}$$

Finally, the impact of the vortex on the flapping moment is needed. Again only the mean and 1/rev part is retained.

$$\Delta\overline{M_\beta}(\lambda_V) = -\frac{1}{2}\int_A^B rV_T\lambda_V dr$$

$$= -\frac{\lambda_{V0}}{2}\left(\int_A^B ra_{V0}\,dr + \int_A^B rb_{V1}\,dr\sin\psi\right) \quad (18)$$

The solution of the integral is given in Appendix A3. Inserting the flapping perturbations of Eq. (6) into Eq. (7) and the aerodynamic moments of Eqs. (15) to (18) on the right side the harmonic balance method can be applied, leading to a system of linear equations for the flapping coefficients. The change of thrust and induced velocity is automatically obtained.

## 3. RESULTS

### 3.1. Bo105: controls required to maintain trim

The following results were calculated with the helicopter rotor model described in Section 2.2. In HOST computations the vortex axis has a remaining 5 deg orientation misalignment with respect to the $x$-axis, thus generating a slight aerodynamic pitching moment. HOST results are compared with the analytical rotor model and with S4 results for the cases A, B and D of Table 2, based on the velocity profiles shown in Fig. 4.

Fig. 5 shows the perturbations of the main rotor trim control angles caused by the vortex. Fig. 5 (a) gives results for the 3 MW WT, (b) for the 7 MW WT and (c) for the B-747 vortex. The vortex location relative to the rotor hub ranges from $y_0 = -2$ to $+2$, i.e. from the far left side to the far right side. The agreement of HOST, S4 and the analytical model is excellent.

*Collective control:* For vortex positions in the left half of the rotor ($y_0 < 0$) a positive collective control angle is needed to compensate the vortex induced downwash that dominates over the rotor disk. When the vortex core is at the rotor hub ($y_0 = 0$) the collective control angle is nearly zero because the downwash on the left side equals the upwash on the right side. Vortex positions on the right side of the rotor require negative collective control angle because the vortex-induced upwash dominates over the rotor disk.

Comparing Fig. 5 (a), (b) and (c) the 7 MW turbine causes larger perturbations in control angles than the 3 MW turbine and the B-747 vortex requires about 4 times more control angle employed than in case of the 7 MW WT. This is due to the increasing circulation strength from case A to D.

*Longitudinal rotor control angle* $\Delta\theta_S$*:* Due to the vortex orientation relative to the rotor the resulting aerodynamic roll moments cause changes in the longitudinal control angle to cancel the vortex impact on trim. The plot shows the biggest changes when the vortex is located at $y_0 = -1$, 0 and +1.

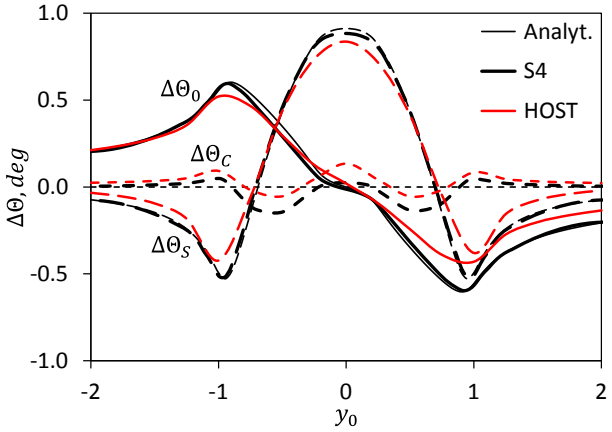


( a ) Case A: 3 MW WT

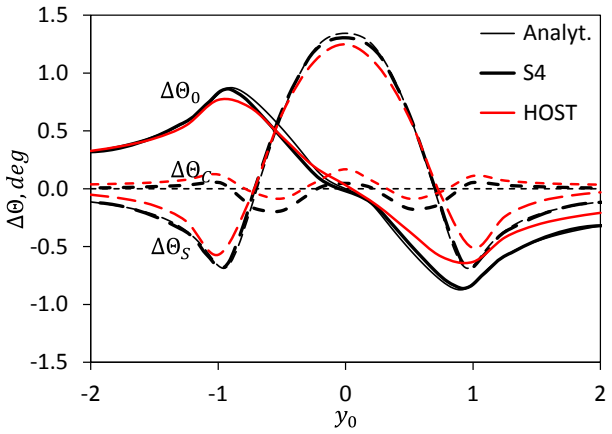


( b ) Case B: 7 MW WT

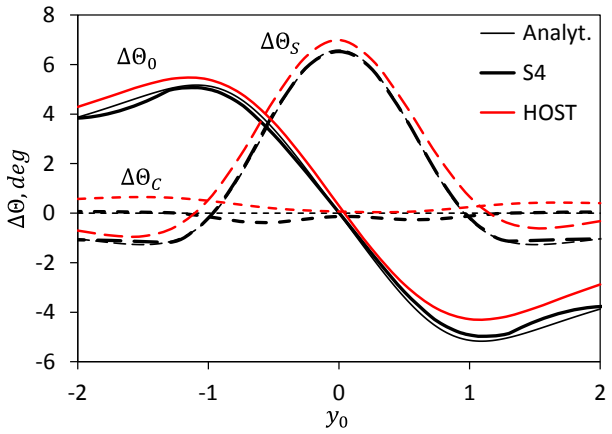


( c ) Case D: B-747

**Fig. 5:** Vortex impact on rotor control angles, hover.

A vortex position at the rotor hub ($y_0 = 0$) generates as much downwash on the right side of the rotor as upwash on the left side. Then, a positive aerodynamic roll moment appears and needs to be compensated by a positive longitudinal control angle.

When the vortex is located at either end of the rotor disk the longitudinal control angle needed to compensate its influence is negative in both cases. This is due to the vortex-induced velocity gradients within the rotor disk. For $y_0 = -1$ the entire disk is immersed in downwash of the vortex, with largest val-

ues on the left side of the disk, thus a positive gradient from left to right. For $y_0 = +1$ the entire disk is immersed in upwash of the vortex, with largest values on the right side of the disk, thus again a positive gradient from left to right. Therefore, in both cases a negative longitudinal control is needed to compensate this gradient.

*Lateral control angle* $\Delta\theta_C$*:* From simple considerations due to the setup of the problem no perturbations are expected, since the vortex does not introduce a longitudinal velocity gradient within the rotor disk. This is also the result of the analytical model. However, the non-linear simulation codes HOST and S4 both compute a small lateral control angle.

All controls shown in Fig. 5 that are required to compensate the WT wake vortex effects are small to moderate, compared to an available control bandwidth of approximately 8 deg. A rotor control ratio (RCR) can be established that relates the required maximum control angle to the available control angle. Similarly, a rotor flapping ratio (RFR) can be defined, relating the maximum flapping perturbation angle to the maximum allowed flapping angle, which is about 15 deg for the Bo105.

$$RCR = \frac{\left|\Delta\Theta_0\right| + \sqrt{\Delta\Theta_S^2 + \Delta\Theta_C^2}}{\Delta\Theta_{max}} \qquad (19)$$

$$RFR = \frac{\left|\Delta\beta_0\right| + \sqrt{\Delta\beta_S^2 + \Delta\beta_C^2}}{\Delta\beta_{max}}$$

For the cases of Fig. 5 these ratios are given in Fig. 6. As long as the vortex center is outside to the right or left of the rotor disk its influence on blade flapping is small due to small vortex-induced velocities. For small vortex core radii relative to the rotor radius, which is in effect for cases A and B, the maximum RCR is obtained when the vortex axis is located close to the right and left end of the disk, see Fig. 6 (a) and (b), because the largest influence on collective is combined with a large influence on cyclic control, as seen in Fig. 5 (a) and (b).

Moving the vortex center more inboard reduces its influence on the collective and the cyclic control angles quickly approaches zero, thus the RCR correspondingly becomes smaller. When the vortex is centered in the disk, its influence on collective control is zero, but the largest influence on cyclic control is present, again leading to a local maximum RCR.

Although the general behavior is similar for large vortex core radius relative to the rotor radius as is present in case D, the induced velocity gradients becomes smaller, see Fig. 4. This reduces the vortex influence on cyclic control for positions close to the right and left end of the disk as shown in Fig. 5 (c), while the influence on cyclic flapping for central positions within the disk remains large. In this case, Fig. 5 indicates an almost linear vortex-induced velocity across the disk. Therefore, the maximum RCR for large vortex core radii is found for vortex positions close to the center of the rotor disk and not at the right or left end of it, see Fig. 6 (c).

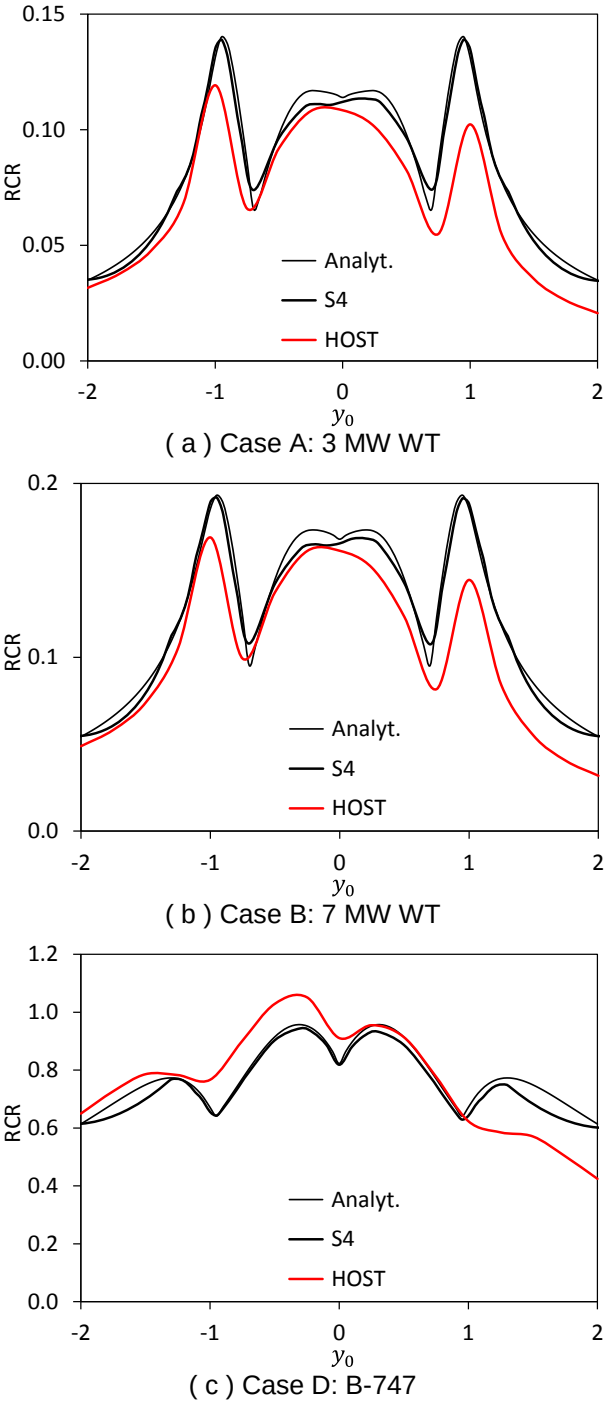


**Fig. 6:** Rotor control ratio in hover.

Finally, the change in rotor power is of interest, because it must be expected that such an aerodynamic disturbance causes a large variety of angles of attack and thus will modify both the induced drag and the airfoil drag. Results are given in Fig. 7 for the

same cases as before. Due to re-trimming the rotor for constant thrust the changes in thrust and thrust-induced velocity are zero. Only in HOST a slight deviation of thrust-induced velocity is resulting; the reason for this has to be investigated.

When the vortex is on the left of the rotor the induced downwash increases and with it the power required, as if it is in a climb. At positions on the right side of the rotor vortex-induced upwash acts like a descent flight and thus reduces the power required.

It may be somewhat surprising that vortex positions around the rotor center $-0.5 < y_0 < -0.3$ cause a reduction of rotor power for cases A and B (vortex core radius small relative to rotor radius, Fig. 7 (a) and (b), while large core radii as in Fig. 7 (c) do not show an influence on the power for a center position of the vortex. This effect may be explained with the highly nonlinear velocity profile within the rotor disk of the small core radius vortices, see Fig. 4. Obviously the induced drag reduction on the upwash side of the vortex core "outperforms" the increased induced drag on the downwash side of it.

This effect is not present for large vortex core radius relative to the rotor radius as seen in Fig. 7 (c). The vortex-induced velocity profile for a central vortex position within the rotor disk is almost linear across it, thus the reduction of induced drag on the upwash side is balanced by the increase of it on the downwash side and the integral effect on power is zero.

### 3.2. Bo105: vortex-induced blade flapping

The rotor first is trimmed in undisturbed atmosphere, then the controls are kept fixed and thereafter the vortex is introduced without re-trimming the rotor. In this case rotor blade flapping perturbations will develop in coning and 1/rev. Higher harmonics are not considered here, but will emerge as well. Cases A, B and D as before are investigated.

The hingeless rotor type of the Bo105 with a natural frequency of flapping of $\nu_\beta = 1.12/rev$ has a phase lag of about 72 deg in 1/rev flapping, in contrast to a centrally hinged teetering rotor with $\nu_\beta = 1.0/rev$ and 90 deg phase lag. Therefore, the blade response to a pure Sine excitation of the vortex will develop both a major Cosine and a smaller Sine component in blade flapping.

This is clearly visible in Fig. 8, and the longitudinal and lateral flapping angles follow the behavior of the longitudinal control shown in Fig. 5 with about the same magnitude. The arcus tangent of the ratio of longitudinal and lateral flapping yields a phase of 72 deg as expected and the results of the analytical model, the isolated rotor code S4 and of the complete helicopter simulation – used in isolated rotor mode – are in surprisingly good agreement.

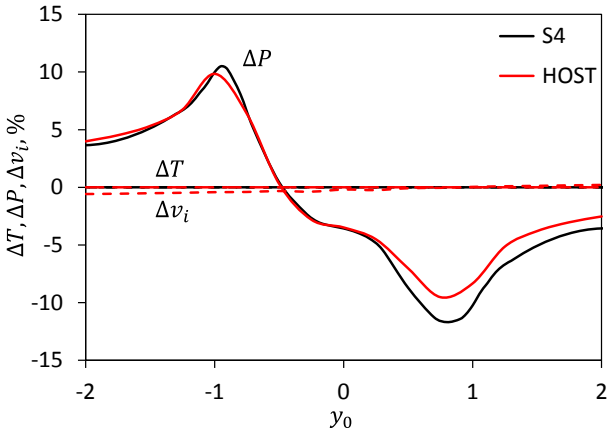

( a ) Case A: 3 MW WT

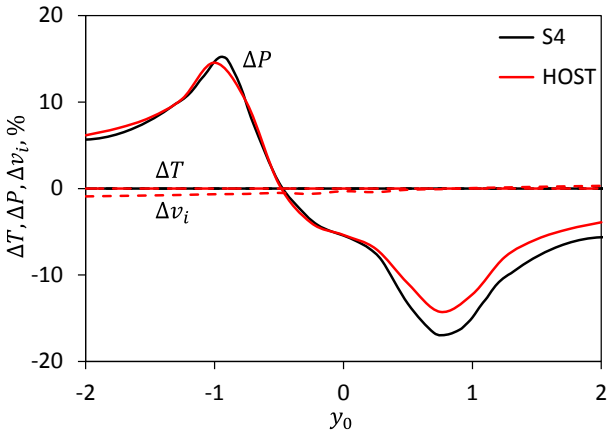

( b ) Case B: 7 MW WT

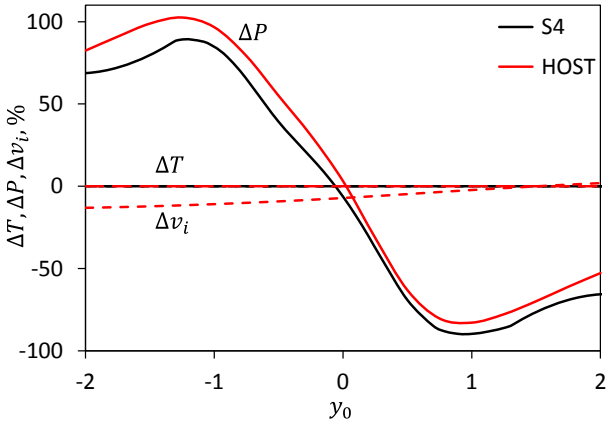

( c ) Case D: B-747

**Fig. 7:** Vortex impact on rotor power in hover.

The blade coning correlates well with the collective of Fig. 7, but with less magnitude. This is due to the balance of the centrifugal forces due to blade mass and the blade lift. Here the blade Lock number $\gamma$ has a great influence, representing the ratio of blade inertia to aerodynamic moments. Light-weight blades will have a larger coning because the centrifugal forces are less, and heavy blades will have less coning due to the opposite.

As observed before in the control angles required and the RCR, a large vortex core radius relative to

the rotor radius such as in case D shown in Fig. 8 (c) has less impact on blade flapping for vortex positions near the edges of the disk.

For the same reasons outlined in description of Fig. 5 the largest influence of the vortex on cyclic flapping is found for the central position within the disk, while the largest coning is developing when the vortex center is outside the disk such that the maximum amount of upwash or downwash affects the blade lift.

In parallel to the rotor control ratio (RCR) that reflects the ability of the pilot to counteract the vortex impact on trim, a rotor flapping ratio (RFR) reflects how much flapping evolves before the blades will collide with the tail boom or the blade stops at the mast. The Bo105 has a relative large amount of allowed flapping of about 15 deg, before the rotor blades collide with the tail boom or the end plates of the horizontal stabilizer. The results for the RFR are given in Fig. 9. Due to the large amount of allowed flapping the ratios are small and considered as uncritical.

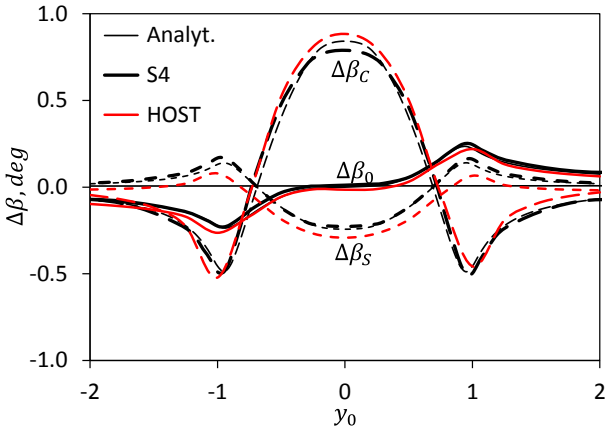


( a ) Case A: 3 MW WT

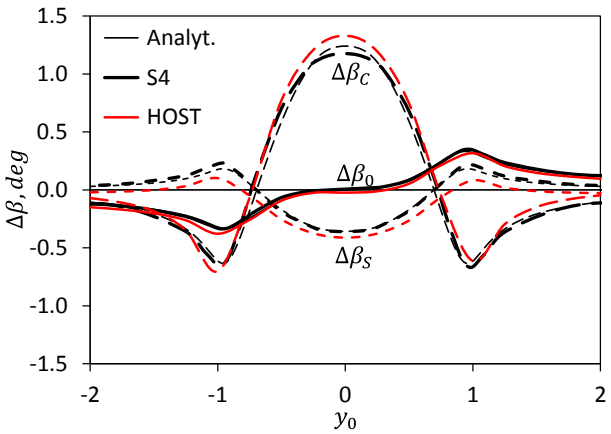


( b ) Case B: 7 MW WT

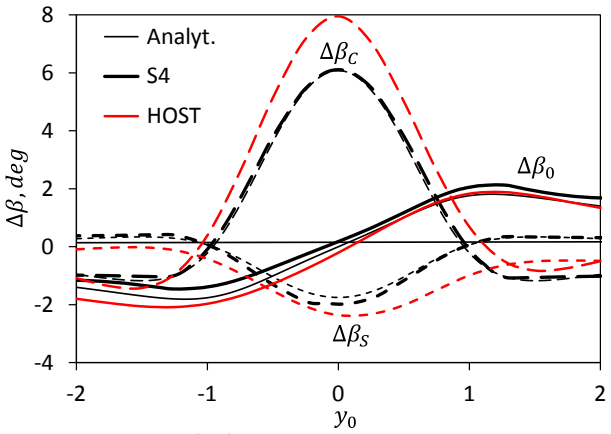


( c ) Case D: B-747

**Fig. 8:** Vortex impact on flapping angles, hover.

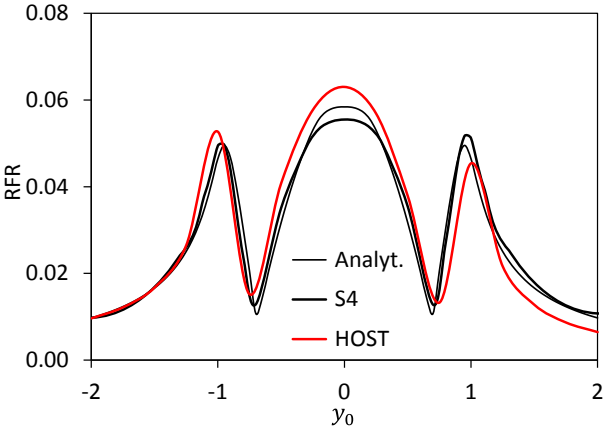


( a ) Case A: 3 MW WT

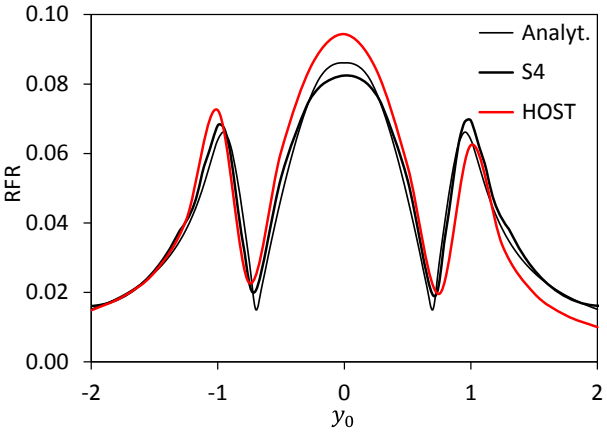


( b ) Case B: 7 MW WT

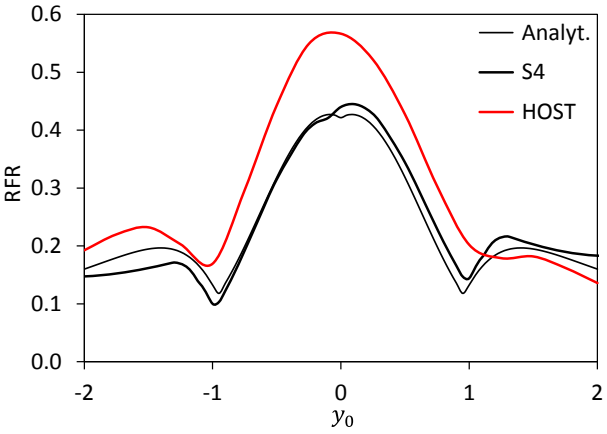


( c ) Case D: B-747

**Fig. 9:** Rotor flapping ratio in hover.

Not re-trimming the rotor causes the rotor thrust and moments to vary from the undisturbed trim, and therefore induced velocities and power will vary accordingly. This is shown in Fig. 10, to be compared to the case of re-trimming the rotor in Fig. 7. Thrust and with it the thrust-induced velocity varies with the vortex-induced mean velocity acting on the rotor disk. The behavior of the power, however, is very different from the re-trimmed case. A power reduction is found for almost all vortex positions.

Vortex positions on the left side of the rotor it mainly induces downwash, reducing the rotor thrust, the mean thrust-induced velocity and thus the major part of rotor induced power. When the vortex is on the right side of the rotor disk it mainly induces upwash, increasing rotor thrust and with it the mean thrust-induced velocity. In this case the vortex-induced upwash and the thrust-induced downwash are acting against each other.

When the vortex is outside to the right side of the rotor disk both influences cancel each other and the power remains virtually unchanged.

### 3.3. Analytical model applied to other rotors

In the foregoing investigations the analytical model is found in excellent agreement with the more sophisticated rotor codes.

Therefore (and because the further rotorcraft listed in Table 3 are not modeled in S4 or in HOST), the rotor controls required to compensate vortex effects on trim (in case of helicopters only) and the vortex influence on blade flapping (including the autogyro) are computed for cases A-D. For the small UL rotorcraft with teetering rotor systems it is of interest whether mast bumping can happen due to excessive flapping (especially for AGs and 2-bladed single rotor helicopters), or blade collisions (in case of coaxial rotors).

In the following only the RCR and the RFR are shown for the various types of rotors listed in Table 3, exposed to the cases of Table 2. The effect of vortices generated by WTs of 3, 7, and 10 MW power (cases A to C) and that of a large fixed-wing aircraft (case D) on the rotor control ratio in dependence on the lateral vortex position within the rotor disk is shown in Fig. 11. It is obvious that for increasing size and weight of the rotorcraft the amount of control to mitigate the vortex effects on rotor trim will be reduced.

The most critical RCR are thus found for the smallest vehicle, the ultralight COAX helicopter, Fig. 11 (a). Even the large WT vortices require close to 50% of the available (assumed) control margin, and the large aircraft vortex exceeds it, causing uncontrollable reactions of the vehicle.

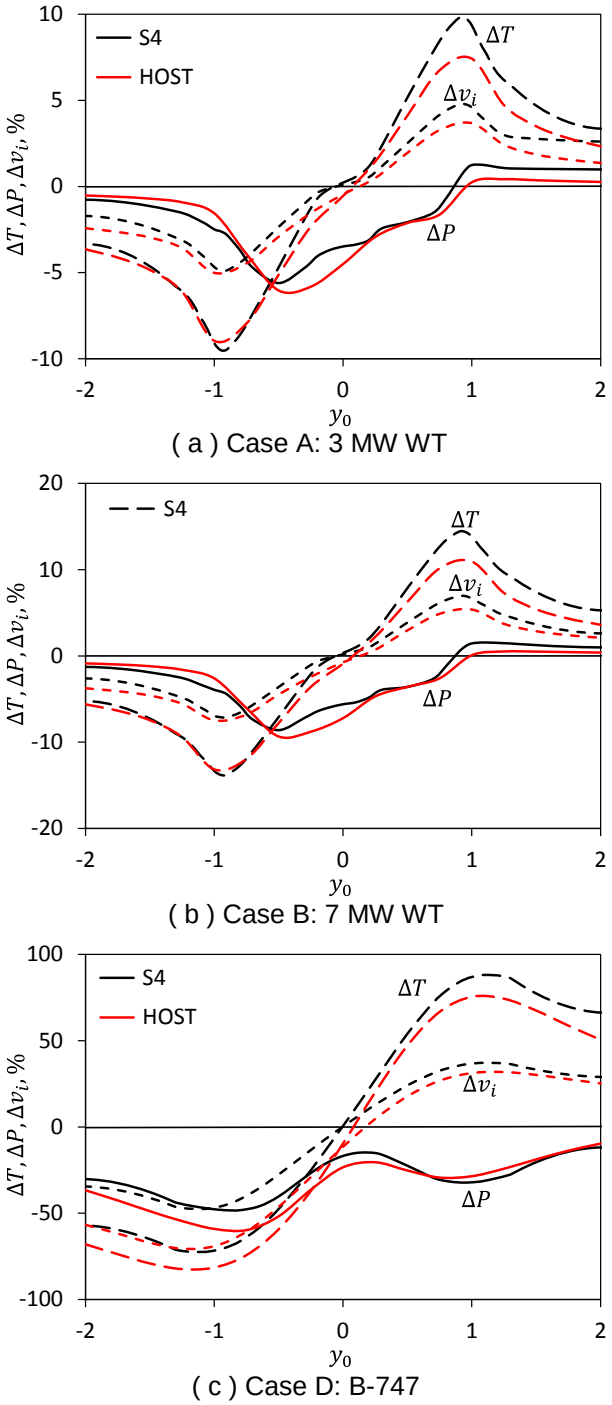


**Fig. 10:** Vortex impact on rotor power in hover.

For the next larger helicopter, the Bo105 shown in Fig. 11 (b), the effects are reduced, but the large aircraft vortex requires almost the full amount of available control to keep the rotor trim constant. The much larger UH-1D and the even larger CH-53D are both less affected, but still the large aircraft vortex requires up to 80% of the available control margin Fig. 11 (c) and (d). The WT vortices appear to be no problem for all helicopters of size Bo105 and up, requiring up to 25% (Bo105) to 15% (CH-53D) of the control margin.

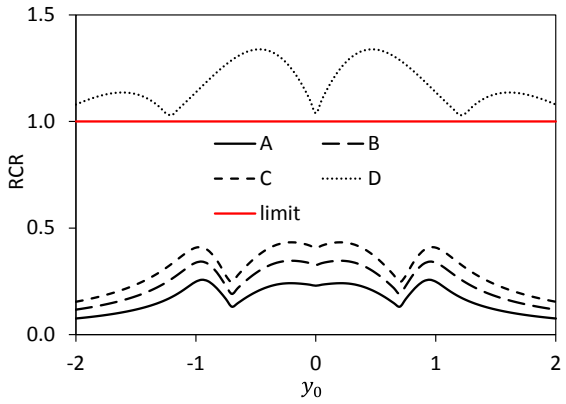


( a ) ultralight COAX helicopter

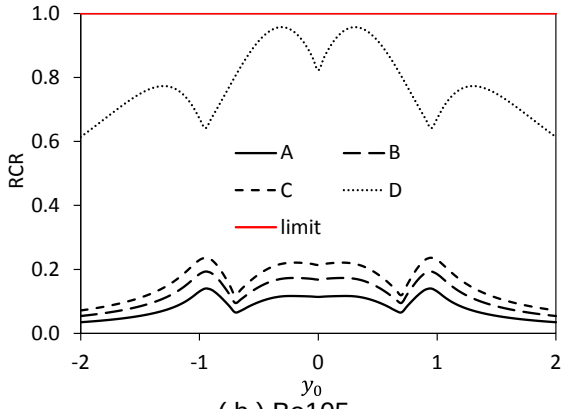


( b ) Bo105

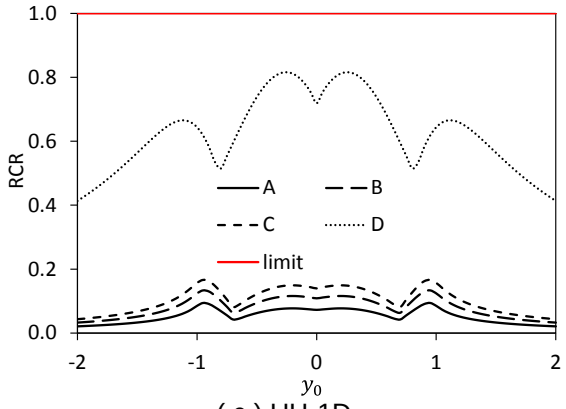


( c ) UH-1D

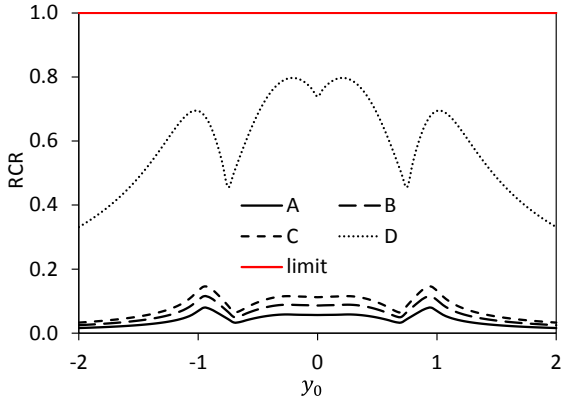


( d ) CH-53D

**Fig. 11:** Rotor control ratios for different helicopters exposed to WT and fixed-wing vortices.

The influence of the same vortices on the rotor blade flapping in terms of the RFR of the same helicopters as in Fig. 11, and additionally on the ultralight autogyro, are given next in Fig. 12.

Note that every rotorcraft has different allowed range of flapping, in contrast to the control margin of the helicopters, which was assumed to 8 deg for all (Table 3). In single rotor teetering blade articulation the maximum allowed flapping may be limited by either mast bumping, which is a catastrophic event with usually rotor separation as the consequence of it, or by blade collision with the tail boom or other elements of the fuselage or empennage.

The major problem of coaxial rotors is a blade collision occurring when blades are flapping in opposite directions. This is especially the case in vortex-rotor interactions, because – for example – the vortex upwash will act on the advancing side of one of the rotors and simultaneously on the retreating side of the other, causing differential harmonic flapping motion. Such differential flapping is the cause of the vertical rotor separation distance, which typically amounts to 20% of the rotor radius.

Mast bumping – or fuselage/tail boom/empennage contact – may be a limit of flapping only in cases where both rotor disks tilt parallel to each other. It must be kept in mind that in the following results it is assumed that the trim condition does not have any 1/rev flapping. If this is not the case the flapping margin is reduced by the amount of flapping already present in the trim state. In trimmed steady state flight the blade flapping of an autogyro can already amount up to 3.5 deg, and even more at lower RPM or during a maneuver [21].

RFR results for the autogyro are given in Fig. 12 (a). Mast bumping is occurring only during interactions with the fixed wing vortex at central positions of it. WT vortices cause blade flapping of 20 to 40% of the available margin (7 deg, see Table 3). However, taking into account the flapping during normal steady state flight the remaining margin for flapping motion becomes only half of that value, doubling the RCR. In addition, operating the rotor at lower RPM or during a maneuver the remaining margin for flapping is even further reduced and then even WT vortices may become a hazard for autogyros.

In contrast to autogyros the RPM of helicopters is fixed within rather small bounds. The RFR results for the ultralight COAX helicopter are given in Fig. 12 (b). It may be surprising that the RFR are generally larger than for the autogyro shown in (a). This is partly caused by the smaller rotor radius and thus larger relative influence of the vortex, see Fig. 4, but mainly due to a smaller flapping margin for the critical case of blade collision, see Table 3.

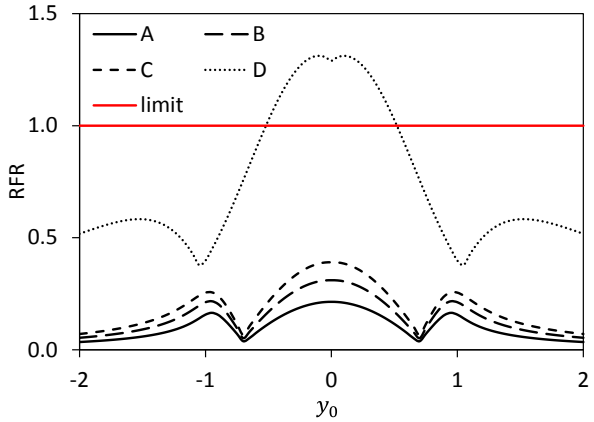


( a ) ultralight autogyro

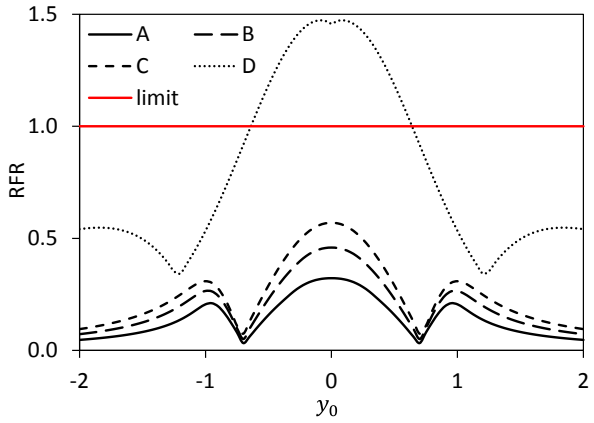


( b ) ultralight COAX helicopter

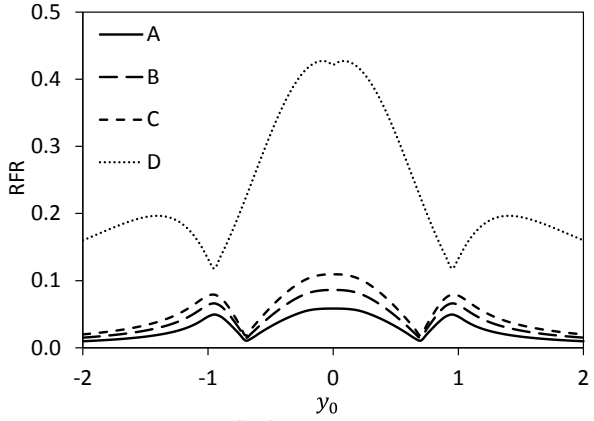


( c ) Bo105

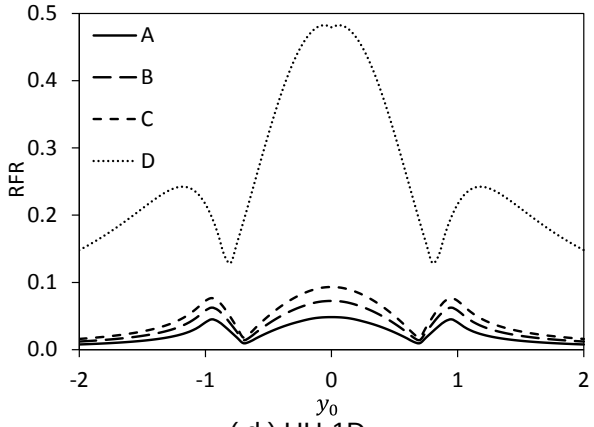


( d ) UH-1D

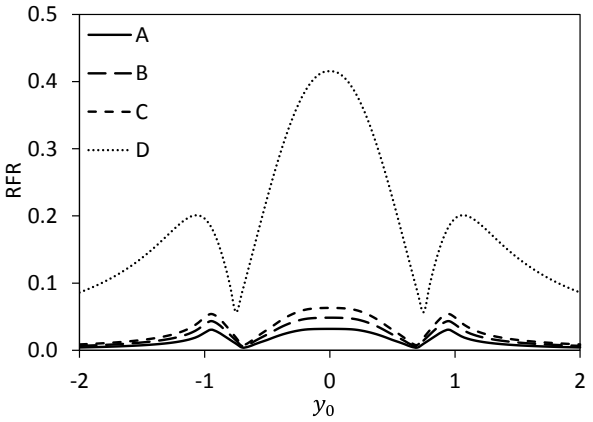


( e ) CH-53D

**Fig. 12:** Rotor flapping ratios for different helicopters exposed to WT and fixed-wing vortices.

Again the fixed wing vortex is the most severe hazard, causing blade collisions for a wide range of vortex positions inside the rotor disk. WT vortices cause RFR between 0.3 and almost 0.6. This may not be critical as such, but some differential flapping will occur during normal flight as well, reducing the available margin and increasing further the RFR. For all other larger helicopters such as the Bo105, the UH-1D and the CH-53D results are shown in Fig. 12 (c)-(e), respectively. These rotorcraft have a significantly higher blade tip speed and larger margins of blade flapping, see Table 3, and thus less influence of the WT or fixed wing vortices, as was already demonstrated in Fig. 5. Consequently the RFR is significantly less than for the ultralight rotorcraft discussed before. The maximum RFR of almost 0.5 is found for the UH-1D in Fig. 12 (d), and less for the Bo105 and the CH-53D. The RFR due to WT vortices range around 0.1 and are considered as not of importance.

### 3.4. Bo105: forward flight

The effect of forward flight at an advance ratio (for zero shaft angle of attack) of $\mu$ = 0.3 is investigated next at the example of the Bo105 rotor and for case B only. Again results of the analytical model are compared with those of the S4 and HOST codes. First the vortex effect on the rotor thrust and hub moments is compensated by rotor controls, Fig. 13.

In Fig. 13 (a) the general form of collective and cyclic controls as a function of lateral vortex position is shown, to be compared with those in hover given in Fig. 5 (b). The overall appearance is similar as in hover, but asymmetric in forward flight. Vortex position at the edge of the rotor disk on the retreating side cause larger disturbances in terms of angle of attack due to smaller tangential velocities at the blade elements, thus larger cyclic and with it larger collective controls than in hover are required. Contrary, vortex positions at the edge on the advancing

side are less disturbing due to the larger tangential velocities there, compared to hover. Inboard positions on the advancing side again have a slightly larger impact on controls than in hover. The consequences of these are reflected in the RCR given in Fig. 13 (b), to be compared with Fig. 6 (b): an asymmetry is clearly visible and the maximum RCR are larger than in hover. Fig. 13 (c) shows the impact on power required, to be compared with Fig. 7 (b). Again, the aforementioned asymmetry is found.

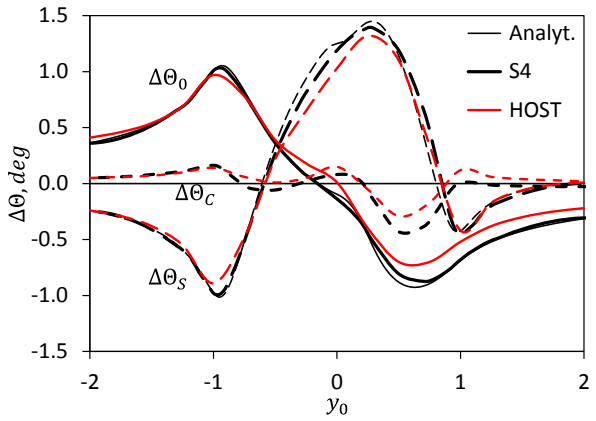


( a ) Vortex impact on rotor control angles

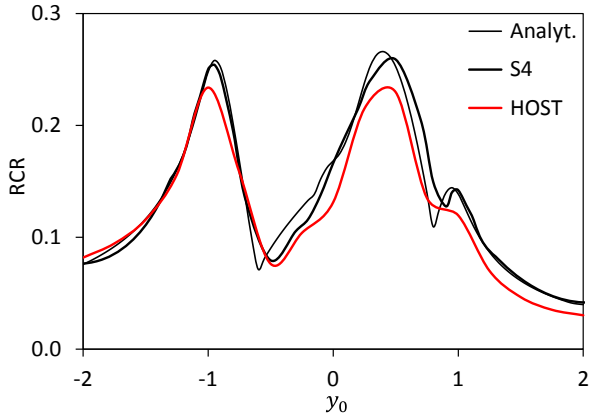


( b ) Rotor control ratio

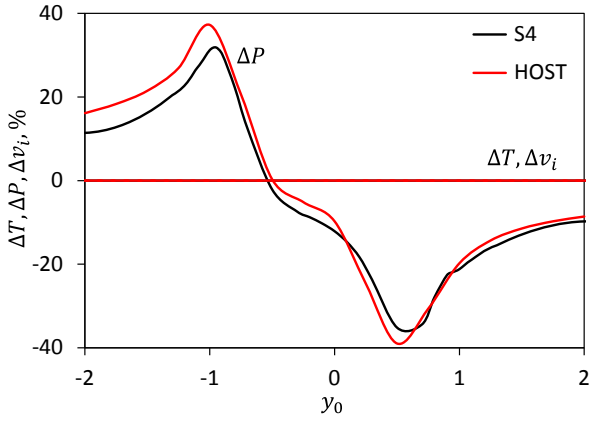


( c ) Vortex impact on rotor power

**Fig. 13:** Rotor controls required for vortex disturbance rejection and power in forward flight, case B.

The maximum power increase is 30% (in hover: 15%) of the undisturbed trim power and the maximum decrease is about -35% (versus -17% in hover). This is caused by vortex upwash or downwash, felt by the rotor as an equivalent to a climb or descent situation, respectively.

The vortex impact on a rotor without re-trimming is shown next in Fig. 14 (a) with respect to rotor blade flapping, to be compared with Fig. 8 (b) for the hovering case. The asymmetry already found in the controls is found again, but with larger flapping response for vortex positions on the advancing side and less on the retreating side. This is due to the larger dynamic pressure and associated aerodynamic forces acting on the blade, compared to those on the retreating side.

Consequently the RFR in Fig. 14 (b) is largest for vortex positions on the advancing side edge of the disk, while in hover it is largest for central vortex positions. Finally the impact on thrust, thrust-induced velocity and rotor power is shown in Fig. 14 (c), to be compared with Fig. 10 (b) in hover. The percentage change in power and induced velocity is virtually the same, and amounts to an increase of up to 23% thrust and induced velocity for vortex positions at the advancing side edge of the disk, versus 15% in hover. The loss of thrust for positions on the retreating side edge of the disk is about the same as in hover.

However, the resulting change of power required shown in Fig. 14 (c) is different from the hovering case Fig. 10 (b). The vortex positions on the retreating side of the disk, especially close to the edge of it and outside, now cause a power increase versus a decrease in hover. In this forward flight condition the vortex-induced peak velocities are larger than the thrust-induced velocities, which appear vice-versa in the hovering case, and therefore causing the reversal of the impact on power. Overall, the analytical model results are very close to those obtained with more sophisticated codes.

## 4. CONCLUSIONS

In this paper the effect of a young wake vortex generated by wind turbines (WT) 100 m behind them and by a large fixed-wing aircraft (2000 m behind it) on the rotor control ratio (RCR) as well as on the rotor flapping ratio (RFR) is presented. Rotors considered range from ultralight rotorcraft (autogyro and coaxial helicopter), to small, medium and large helicopters. Results from the Bo105 helicopter rotor simulated by HOST are compared with those obtained by a simplified analytical treatment of an isolated rotor, and those of DLR's isolated rotor code S4.

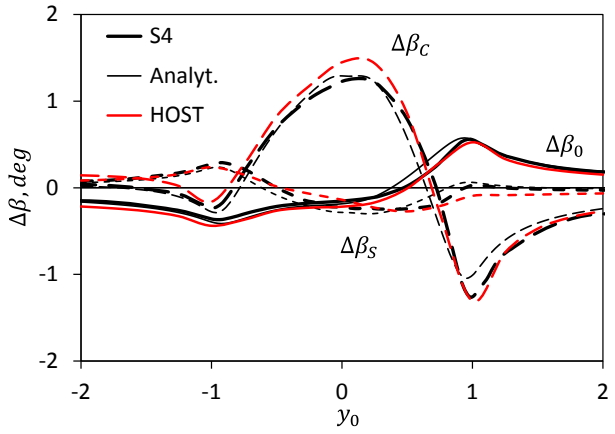


( a ) Vortex impact on flapping angles

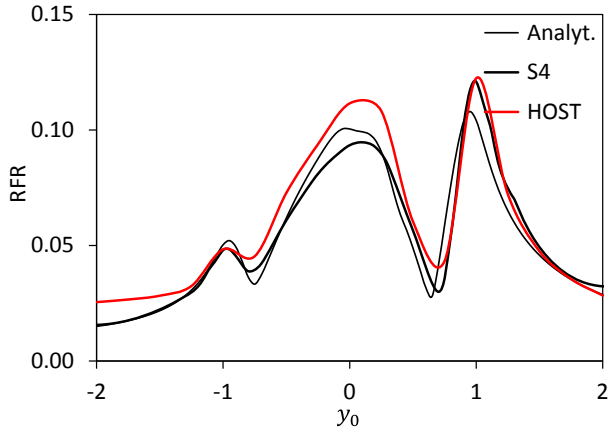


( b ) Rotor flapping ratio

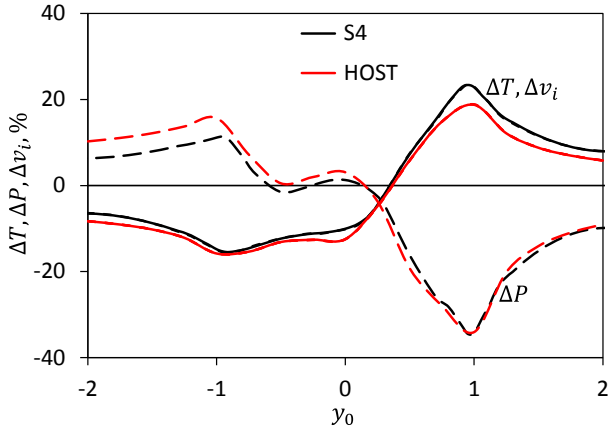


( c ) Vortex impact on rotor power

**Fig. 14:** Vortex-induced blade flapping and influence on power and thrust in forward flight, case B.

The major conclusions are:

- The simplified isolated rotor analysis generates results very close to those of the nonlinear sophisticated rotor or complete helicopter codes for this kind of investigation, despite the simplifications made.
- For autogyros WT vortices may become hazardous, because the blade flapping developing in addition to that of the flapping due to the flight condition may result in mast bumping. Large aircraft vortices are always dangerous for autogyros.
- Small (Bo105 size), medium and large helicopters are more limited by the available control margin than by the margin of flapping. A large fixed wing aircraft vortex can result in RCR of 1 for the small helicopter, and up to 0.8 for the larger ones, but the RFR for all remains below 0.5 due to a larger flapping margin, compared to the control margin. In any case, the WT vortices are not causing hazardous RCR or RFR for these helicopter sizes.
- Ultralight coaxial helicopters may also be in danger due to the potential of blade collisions, because a vortex encounter results in differential blade flapping that cannot be compensated by pilot control. Big aircraft vortex encounters exceed a RCR of 1, and WT vortices cause a RCR of almost 0.5. The limited amount of differential flapping becomes dangerous in case of a large fixed wing vortex encounter, and the RFR generated by WT vortices may reach 0.6.
- In hover the impact of the vortex on rotor controls, flapping and power are symmetric, while in forward flight they become asymmetric and larger than in hover. In forward flight larger controls are required for re-trimming when the vortex is on the retreating side of the rotor, and larger flapping develops when it is on the advancing side.
- RCR and RFR are larger in forward flight than in hover. However, for the Bo105 example they remain uncritical for the 7 MW WT investigated.
- With no pilot action the vortex-induced velocities modify the small helicopter (Bo105) rotor thrust by up to ±90% in hover, which will cause a significant influence on flight mechanics of the helicopter. In forward flight the change of thrust is much less (±20%).
- The rotor power in these cases is always reduced by up to 50% in hover. In forward flight a power increase up to +20% is found when the vortex generates downwash on the retreating side, and a power decrease of -30% for upwash on the advancing side.
- When re-trimming for constant thrust the rotor power is varying by ±100% in hover and ±40% in forward flight. In the latter a power increase is found when the vortex generates downwash on the retreating side, and a power decrease for upwash on the advancing side.
- All of these effects can be explained with the relation of the magnitude of rotor thrust-induced velocities to the vortex-induced velocities. In hover, the rotor thrust-induced velocities are

larger, while in forward flight the thrust-induced velocities quickly become smaller than the vortex-induced velocities that are independent of the helicopter's flight speed.

Future investigations will focus on the complete helicopter trim when all components of the helicopter are subjected to the vortex, and to the flight dynamics response when entering and leaving the aircraft vortex or the WT wake spiral. This will be investigated for different flight speeds of the helicopter.

## 5. REFERENCES


[1] Dunham, R.E., Holbrook, G.T., Mantay, W.R., Campbell, R.L., Van Gunst, R.W., "Flight-Test Experience of a Helicopter Encountering an Airplane Trailing Vortex", 32nd Annual National V/STOL Forum of the American Helicopter Society, Washington, DC, May 10-12, 1976.

[2] Mantay, W.R., Holbrook, G.T., Campbell, R.L. and Tamaine, R.L., "Helicopter response of an airplane's trailing vortex," *Journal of Aircraft*, **14**(4), 1977, pp. 357-363.

[3] Saito, S., Azuma, A., Kawachi, K., Okuno, Y., Hasegawa, T., "Numerical simulations of dynamic response of fixed and rotary wing aircraft to a large airplane wake," 13th European Rotorcraft Forum, Arles, France, Sept. 8-11, 1987.

[4] Azuma, A., Saito, S., Kawachi, K., "Response of a helicopter penetrating the tip vortices of a large airplane," *VERTICA*, **11**(1), 1987, pp. 65-76.

[5] Turner, G.P., Padfield, G.D., Harris, M., "Encounters with Aircraft Vortex Wakes; The Impact on Helicopter Handling Qualities," *Journal of Aircraft*, **39**(5), 2002, pp. 839–849.

[6] Padfield, G.D., Manimala, B., Turner, G.P., "A Severity Analysis for Rotorcraft Encounters with Vortex Wakes," *Journal of the American Helicopter Society*, **49**(4), 2004, pp. 445–456.

[7] Lawrence, B., Padfield, G.D., "Wake Vortex Encounter Severity for Rotorcraft in Approach and Landing," 31st European Rotorcraft Forum, Florence, Italy, Sept. 13-15, 2005.

[8] Whitehouse, G.R., Brown, R.E., "Modeling the Mutual Distortions of Interacting Helicopter and Aircraft Wakes," *Journal of Aircraft*, **40**(3), 2003, pp. 440-449.

[9] Whitehouse, G.R., Brown, R.E., "Modelling a helicopter rotor's response to wake encounters," *The Aeronautical Journal*, **108**(1079), 2004, pp. 15-26.

[10] van der Wall, B.G., Fischenberg, D., Lehmann, P.H., van der Wall, L.B., "Impact of Wind Energy Rotor Wakes on Fixed-Wing Aircraft and Helicopters," 42nd European Rotorcraft Forum, Lille, France, Sept. 5-8, 2016

[11] van der Wall, B.G., van der Wall, L.B., "Analytical Estimate of Rotor Controls Required for a Straight Vortex Disturbance Rejection," *Journal of the American Helicopter Society*, **62**(1), 2017, pp. 015001-1-4

[12] Leishman, J.G., *Principles of Helicopter Aerodynamics*, Cambridge: Cambridge University Press, UK, 2000.

[13] Burnham, D.C., Hallock, J.N., "Chicago Monostatic Acoustic Vortex Sensing System," U.S. Department of Transportation, DOT-TSC-FAA-79-103, 1982.

[14] Vatistas, G.H., Kozel, V., Mih, W.C., „A Simpler Model for Concentrated Vortices," *Experiments in Fluids*, **11**(1), 1991, pp. 73-76.

[15] Wang, X., White, M., Barakos, G., Wind Turbine Wake Encounter Study. Liverpool: University of Liverpool, UK, 2015.

[16] Benoit, B., Dequin, A.-M., Kampa, K., von Grünhagen, W., Basset, P.-M., Gimonet, B., „HOST, a General Helicopter Simulation Tool for Germany and France", 56th Annual Forum of the American Helicopter Society, Virginia Beach, VA, May 2-4, 2000.

[17] Oseen, C.W., "Über Wirbelbewegung in einer reibenden Flüssigkeit," *Arkiv för Matematik, Astronomi och Fysik*, **7**, 1912, pp. 14-21.

[18] Lamb, H., *Hydrodynamics*, Cambridge: Cambridge University Press, UK, 1932, pp. 592-593, 668-669.

[19] Meijer-Drees, J., "A Theory of Airflow Through Rotors and its Application to Some Helicopter Problems," *Journal of the Helicopter Association of Great Britain*, **3**(2), 1949, pp. 79-104

[20] van der Wall, B.G., Lim, J.W., Smith, M., Jung, S.N., Bailly, J., Baeder, J.D., Boyd, D.D., "The HART II International Workshop: An Assessment of the State-of-the-Art in Comprehensive Code Prediction, *CEAS Aeronautical Journal*, **4**(3), 2013, pp. 223-252

[21] Duda, H., Seewald, *J., Flugphysik der Tragschrauber*, Berlin: Springer Vieweg, 2016

**APPENDIX**

The integral in Eq. (18), based on the kernel function of Eq. (8), is given here in A3, together with the integrals of Eqs. (11) and (12) that have already been presented in [10]. To simplify the expressions of the results the following abbreviations are used.

(20) $$\xi = r^2 - |y_0|^2 + |r_c|^2 \qquad \eta = 2|y_0||r_c|$$

**A1. Radial integration of the coefficient $a_{V0}$**

(21) $$\int a_{V0}\,dr = \mu \ln\sqrt{\sqrt{\zeta^2+\eta^2}+\zeta+2y_0^{\,2}} + \mu \ln\left(1+\frac{\sqrt{2}\,|r_c|}{\sqrt{\sqrt{\zeta^2+\eta^2}+\zeta}}\right) + y_0\frac{\sqrt{2}\,|r_c|}{\sqrt{\sqrt{\zeta^2+\eta^2}+\zeta}}$$

**A2. Radial integration of the product $rb_{V1}$**

(22)
$$\begin{aligned}\int rb_{V1}\,dr &= 2\mu\,\mathrm{sgn}(y_0)|r_c|\arctan\frac{\sqrt{2}\,|y_0|}{\sqrt{\zeta^2+\eta^2}+\zeta}\\ &+ 2\mu y_0\left[\ln\sqrt{\sqrt{\zeta^2+\eta^2}+\zeta+2y_0^{\,2}} + \ln\left(1+\frac{\sqrt{2}\,|r_c|}{\sqrt{\sqrt{\zeta^2+\eta^2}+\zeta}}\right)\right]\\ &+ r^2 - \sqrt{2}\left(|r_c|\sqrt{\sqrt{\zeta^2+\eta^2}+\zeta} - |y_0|\sqrt{\sqrt{\zeta^2+\eta^2}-\zeta}\right)\end{aligned}$$

**A3. Radial integration of the product $ra_0$**

(23)
$$\begin{aligned}\int ra_{V0}\,dr &= \mu r + \frac{y_0|r_c|}{\sqrt{2}}\frac{\sqrt{\sqrt{\zeta^2+\eta^2}+\zeta}}{\sqrt{\zeta^2+\eta^2}+\zeta}r\\ &- \frac{y_0+\mu}{2}|r_c|\ln\left[\frac{r\sqrt{2}\sqrt{\sqrt{\zeta^2+\eta^2}+\zeta}+\sqrt{\zeta^2+\eta^2}+r^2}{\sqrt{\left(y_o^2-r_c^2\right)^2+\eta^2}}\right]\\ &- \left(\mathrm{sgn}(y_0)\frac{y_0^2-r_c^2}{2}+\mu|y_0|\right)\arctan\left(\frac{r\sqrt{2}\sqrt{\sqrt{\zeta^2+\eta^2}+\zeta}+\sqrt{\zeta^2+\eta^2}+\zeta}{\eta}\right)\end{aligned}$$